Predicting Depth, Surface Normals and Semantic Labels with a Common Multi-Scale Convolutional Architecture

David Eigen[1] Rob Fergus[1,2]
[1] Dept. of Computer Science, Courant Institute, New York University
[2] Facebook AI Research
{deigen,fergus}@cs.nyu.edu

Abstract

In this paper we address three different computer vision tasks using a single multiscale convolutional network architecture: depth prediction, surface normal estimation, and semantic labeling. The network that we develop is able to adapt naturally to each task using only small modifications, regressing from the input image to the output map directly. Our method progressively refines predictions using a sequence of scales, and captures many image details without any superpixels or low-level segmentation. We achieve state-of-the-art performance on benchmarks for all three tasks.

1. Introduction

Scene understanding is a central problem in vision that has many different aspects. These include semantic labels describing the identity of different scene portions; surface normals or depth estimates describing the physical geometry; instance labels of the extent of individual objects; and affordances capturing possible interactions of people with the environment. Many of these are often represented with a pixel-map containing a value or label for each pixel, *e.g.* a map containing the semantic label of the object visible at each pixel, or the vector coordinates of the surface normal orientation. 矢量坐标

In this paper, we address three of these tasks, depth prediction, surface normal estimation and semantic segmentation — all using a single common architecture. Our multiscale approach generates pixel-maps directly from an input image, without the need for low-level superpixels or contours, and is able to align to many image details using a series of convolutional network stacks applied at increasing resolution. At test time, all three outputs can be generated in real time (~30Hz). We achieve state-of-the art results on all three tasks we investigate, demonstrating our model's versatility.

There are several advantages in developing a general model for pixel-map regression. First, applications to new tasks may be quickly developed, with much of the new work lying in defining an appropriate training set and loss function; in this light, our work is a step towards building off-the-shelf regressor models that can be used for many applications. In addition, use of a single architecture helps simplify the implementation of systems that require multiple modalities, e.g. robotics or augmented reality, which in turn can help enable research progress in these areas. Lastly, in the case of depth and normals, much of the computation can be shared between modalities, making the system more efficient.

2. Related Work

Convolutional networks have been applied with great success for object classification and detection [19, 12, 30, 32, 34]. Most such systems classify either a single object label for an entire input window, or bounding boxes for a few objects in each scene. However, ConvNets have recently been applied to a variety of other tasks, including pose estimation [36, 27], stereo depth [38, 25], and instance segmentation [14]. Most of these systems use ConvNets to find only local features, or generate descriptors of discrete proposal regions; by contrast, our network uses both local and global views to predict a variety of output types. In addition, while each of these methods tackle just one or two tasks at most, we are able to apply our network to three disparate tasks.

Our method builds upon the approach taken by Eigen *et al.* [8], who apply two convolutional networks in stages in stage:分阶段 for single-image depth map prediction. We develop a more general network that uses a sequence of three scales to generate features and refine predictions to higher resolution, which we apply to multiple tasks, including surface normals estimation and per-pixel semantic labeling. Moreover, we improve performance in depth prediction as well, illustrating how our enhancements help improve all tasks.

Single-image surface normal estimation has been addressed by Fouhey *et al.* [10, 11], Ladicky *et al.* [21], Barron and Malik [3, 2], and most recently by Wang *et al.* [37], the latter in work concurrent with ours. Fouhey *et al.* match to discriminative local templates [10] followed by a global op-

NYUDepth 的尺寸是304x228，KITTI是576x172
本文使用的NYU

timization on a grid drawn from vanishing point rays [11], while Ladicky *et al.* learn a regression from over-segmented regions to a discrete set of normals and mixture coefficients. Barron and Malik [3, 2] infer normals from RGB-D inputs using a set of handcrafted priors, along with illumination and reflectance. From RGB inputs, Wang *et al.* [37] use convolutional networks to combine normals estimates from local and global scales, while also employing cues from room layout, edge labels and vanishing points. Importantly, we achieve as good or superior results with a more general multiscale architecture that can naturally be used to perform many different tasks.

Prior work on semantic segmentation includes many different approaches, both using RGB-only data [35, 4, 9] as well as RGB-D [31, 29, 26, 6, 15, 17, 13]. Most of these use local features to classify over-segmented regions, followed by a global consistency optimization such as a CRF. By comparison, our method takes an essentially inverted approach: We make a consistent global prediction first, then follow it with iterative local refinements. In so doing, the local networks are made aware of their place within the global scene, and can can use this information in their refined predictions.

Gupta *et al.* [13, 14] create semantic segmentations first by generating contours, then classifying regions using either hand-generated features and SVM [13], or a convolutional network for object detection [14]. Notably, [13] also performs amodal completion, which transfers labels between disparate regions of the image by comparing planes from the depth.

Most related to our method in semantic segmentation are other approaches using convolutional networks. Farabet *et al.* [9] and Couprie *et al.* [6] each use a convolutional network applied to multiple scales in parallel generate features, then aggregate predictions using superpixels. Our method differs in several important ways. First, our model has a large, full-image field of view at the coarsest scale; as we demonstrate, this is of critical importance, particularly for depth and normals tasks. In addition, we do not use superpixels or post-process smoothing — instead, our network produces fairly smooth outputs on its own, allowing us to take a simple pixel-wise maximum.

Pinheiro *et al.* [28] use a recurrent convolutional network in which each iteration incorporates progressively more context, by combining a more coarsely-sampled image input along with the local prediction from the previous iteration. This direction is precisely the reverse of our approach, which makes a global prediction first, then iteratively refines it. In addition, whereas they apply the same network parameters at all scales, we learn distinct networks that can specialize in the edits appropriate to their stage.

Most recently, in concurrent work, Long *et al.* [24] adapt the recent VGG ImageNet model [32] to semantic segmentation by applying 1x1 convolutional label classifiers at feature maps from different layers, corresponding to different scales, and averaging the outputs. By contrast, we apply networks for different scales in series, which allows them to make more complex edits and refinements, starting from the full image field of view. Thus our architecture easily adapts to many tasks, whereas by considering relatively smaller context and summing predictions, theirs is specific to semantic labeling.

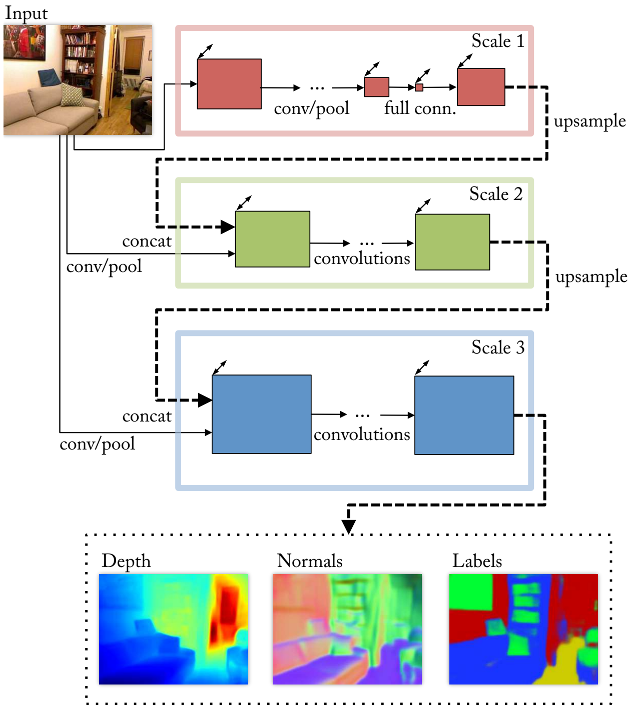

	Layer	1.1	1.2	1.3	1.4	1.5	1.6	1.7	upsamp
Scale 1 (AlexNet)	Size	37x27	18x13	18x13	18x13	8x6	1x1	19x14	74x55
	#convs	1	1	1	1	1	–	–	–
	#chan	96	256	384	384	256	4096	64	64
	ker. sz	11x11	5x5	3x3	3x3	3x3	–	–	–
	Ratio	/8	/16	/16	/16	/32	–	/16	/4
	l.rate	0.001	0.001	0.001	0.001	0.001	see text		
	Layer	1.1	1.2	1.3	1.4	1.5	1.6	1.7	upsamp
Scale 1 (VGG)	Size	150x112	75x56	37x28	18x14	9x7	1x1	19x14	74x55
	#convs	2	2	3	3	3	–	–	–
	#chan	64	128	256	512	512	4096	64	64
	ker. sz	3x3	3x3	3x3	3x3	3x3	–	–	–
	Ratio	/2	/4	/8	/16	/32	–	/16	/4
	l.rate	0.001	0.001	0.001	0.001	0.001	see text		
	Layer	2.1	2.2	2.3	2.4	2.5			upsamp
Scale 2	Size	74x55	74x55	74x55	74x55	74x55			147x109
	#chan	96+64	64	64	64	C			C
	ker. sz	9x9	5x5	5x5	5x5	5x5			–
	Ratio	/4	/4	/4	/4	/4			/2
	l.rate	0.001	0.01	0.01	0.01	0.001			
	Layer	3.1	3.2	3.3	3.4				final
Scale 3	Size	147x109	147x109	147x109	147x109				147x109
	#chan	96+C	64	64	C				C
	ker. sz	9x9	5x5	5x5	5x5				–
	Ratio	/2	/2	/2	/2				/2
	l.rate	0.001	0.01	0.01	0.001				

Figure 1. Model architecture. C is the number of output channels in the final prediction, which depends on the task. The input to the network is 320x240.

3. Model Architecture

Our model is a multi-scale deep network that first predicts a coarse global output based on the entire image area, then refines it using finer-scale local networks. This scheme is illustrated in Fig. 1. While our model was initially based upon the architecture proposed by [8], it offers several architectural improvements. First, we make the model deeper (more convolutional layers). Second, we add a third scale at higher resolution, bringing the final output resolution up to half the input, or 147 × 109 for NYUDepth. Third, instead of passing output *predictions* from scale 1 to scale 2, we pass multichannel *feature maps*; in so doing, we found we could also train the first two scales of the network jointly from the start, somewhat simplifying the training procedure and yielding performance gains.

Scale 1: Full-Image View The first scale in the network predicts a coarse but spatially-varying set of features for the entire image area, based on a large, full-image field of view, which we accomplish this through the use of two fully-connected layers. The output of the last full layer is reshaped to 1/16-scale in its spatial dimensions by 64 features, then upsampled by a factor of 4 to 1/4-scale. Note since the feature upsampling is linear, this corresponds to a decomposition of a big fully connected layer from layer 1.6 to the larger 74 × 55 map; since such a matrix would be prohibitively large and only capable of producing a blurry output given the more constrained input features, we constrain the resolution and upsample. Note, however, that the 1/16-scale output is still large enough to capture considerable spatial variation, and in fact is twice as large as the 1/32-scale final convolutional features of the coarse stack.

Since the top layers are fully connected, each spatial location in the output connects to the all the image features, incorporating a very large field of view. This stands in contrast to the multiscale approach of [6, 9], who produce maps where the field of view of each output location is a more local region centered on the output pixel. This full-view connection is especially important for depth and normals tasks, as we investigate in Section 7.1.

As shown in Fig. 1, we trained two different sizes of our model: One where this scale is based on an ImageNet-trained AlexNet [19], and one where it is initialized using the Oxford VGG network [32]. We report differences in performance between the models on all tasks, to measure the impact of model size in each.

Scale 2: Predictions The job of the second scale is to produce predictions at a mid-level resolution, by incorporating a more detailed but narrower view of the image along with the full-image information supplied by the coarse network. We accomplish this by concatenating the feature maps of the coarse network with those from a single layer of convolution and pooling, performed at finer stride (see Fig. 1). The output of the second scale is a 55x74 prediction (for NYUDepth), with the number of channels depending on the task. We train Scales 1 and 2 of the model together jointly, using SGD on the losses described in Section 4.

Scale 3: Higher Resolution The final scale of our model refines the predictions to higher resolution. We concatenate the Scale-2 outputs with feature maps generated from the original input at yet finer stride, thus incorporating a more detailed view of the image. The further refinement aligns the output to higher-resolution details, producing spatially coherent yet quite detailed outputs. The final output resolution is half the network input.

4. Tasks

We apply this same architecture structure to each of the three tasks we investigate: depths, normals and semantic labeling. Each makes use of a different loss function and target data defining the task.

4.1. Depth

For depth prediction, we use a loss function comparing the predicted and ground-truth log depth maps D and D^*. Letting $d = D - D^*$ be their difference, we set the loss to

$$L_{depth}(D, D^*) = \frac{1}{n}\sum_i d_i^2 - \frac{1}{2n^2}\left(\sum_i d_i\right)^2 + \frac{1}{n}\sum_i[(\nabla_x d_i)^2 + (\nabla_y d_i)^2] \quad (1)$$

这里的i指的是有效的点，排除那些没有标准值的像素

where the sums are over valid pixels i and n is the number of valid pixels (we mask out pixels where the ground truth is missing). Here, $\nabla_x d_i$ and $\nabla_y d_i$ are the horizontal and vertical image gradients of the difference.

Our loss is similar to that of [8], who also use the l_2 and scale-invariant difference terms in the first line. However, we also include a first-order matching term $(\nabla_x d_i)^2 + (\nabla_y d_i)^2$, which compares image gradients of the prediction with the ground truth. This encourages predictions to have not only close-by values, but also similar local structure. We found it indeed produces outputs that better follow depth gradients, with no degradation in measured l_2 performance.

4.2. Surface Normals

To predict surface normals, we change the output from one channel to three, and predict the x, y and z components of the normal at each pixel. We also normalize the vector at each pixel to unit l_2 norm, and backpropagate through this normalization. We then employ a simple elementwise loss comparing the predicted normal at each pixel to the ground truth, using a dot product:

$$L_{normals}(N, N^*) = -\frac{1}{n}\sum_i N_i \cdot N_i^* = -\frac{1}{n}N \cdot N^* \quad (2)$$

where N and N^* are predicted and ground truth normal vector maps, and the sums again run over valid pixels (*i.e.* those with a ground truth normal).

For ground truth targets, we compute the normal map using the same method as in Silberman *et al.* [31], which estimates normals from depth by fitting least-squares planes to neighboring sets of points in the point cloud.

4.3. Semantic Labels

For semantic labeling, we use a pixelwise softmax classifier to predict a class label for each pixel. The final output then has as many channels as there are classes. We use a simple pixelwise cross-entropy loss,

$$L_{semantic}(C, C^*) = -\frac{1}{n}\sum_i C_i^* \log(C_i) \tag{3}$$

where $C_i = e^{z_i}/\sum_c e^{z_{i,c}}$ is the class prediction at pixel i given the output z of the final convolutional linear layer 3.4.

When labeling the NYUDepth RGB-D dataset, we use the ground truth depth and normals as additional input channels. We convolve each of the three input types (RGB, depth and normals) with a different set of $32 \times 9 \times 9$ filters, then concatenate the resulting three feature sets along with the network output from the previous scale to form the input to the next. We also tried the "HHA" encoding proposed by [14], but did not see a benefit in our case, thus we opt for the simpler approach of using the depth and xyz-normals directly. Note the first scale is initialized using ImageNet, and we keep it RGB-only. Applying convolutions to each input type separately, rather than concatenating all the channels together in pixel space and filtering the joint input, enforces independence between the features at the lowest filter level, which we found helped performance.

5. Training

5.1. Training Procedure

We train our model in two phases using SGD: First, we jointly train both Scales 1 and 2. Second, we fix the parameters of these scales and train Scale 3. Since Scale 3 contains four times as many pixels as Scale 2, it is expensive to train using the entire image area for each gradient step. To speed up training, we instead use random crops of size 74x55: We first forward-propagate the entire image through scales 1 and 2, upsample, and crop the resulting Scale 3 input, as well as the original RGB input at the corresponding location. The cropped image and Scale 2 prediction are forward- and back-propagated through the Scale 3 network, and the weights updated. We find this speeds up training by about a factor of 3, including the overhead for inference of the first two scales, and results in about the same if not slightly better error from the increased stochasticity.

All three tasks use the same initialization and learning rates in nearly all layers, indicating that hyperparameter settings are in fact fairly robust to changes in task. Each were first tuned using the depth task, then verified to be an appropriate order of magnitude for each other task using a small validation set of 50 scenes. The only differences are: (*i*) The learning rate for the normals task is 10 times larger than depth or labels. (*ii*) Relative learning rates of layers 1.6 and 1.7 are 0.1 each for depth/normals, but 1.0 and 0.01 for semantic labeling. (*iii*) The dropout rate of layer 1.6 is 0.5 for depth/normals, but 0.8 for semantic labels, as there are fewer training images.

We initialize the convolutional layers in Scale 1 using ImageNet-trained weights, and randomly initialize the fully connected layers of Scale 1 and all layers in Scales 2 and 3. We train using batches of size 32 for the AlexNet-initialized model but batches of size 16 for the VGG-initialized model due to memory constraints. In each case we step down the global learning rate by a factor of 10 after approximately 2M gradient steps, and train for an additional 0.5M steps.

5.2. Data Augmentation

In all cases, we apply random data transforms to augment the training data. We use random scaling, in-plane rotation, translation, color, flips and contrast. When transforming an input and target, we apply corresponding transformations to RGB, depth, normals and labels. Note the normal vector transformation is the inverse-transpose of the worldspace transform: Flips and in-plane rotations require flipping or rotating the normals, while to scale the image by a factor s, we divide the depths by s but multiply the z coordinate of the normals and renormalize.

5.3. Combining Depth and Normals

We combine both depths and normals networks together to share computation, creating a network using a single scale 1 stack, but separate scale 2 and 3 stacks. Thus we predict both depth and normals at the same time, given an RGB image. This produces a 1.6x speedup compared to using two separate models. [1]

6. Performance Experiments

6.1. Depth

We first apply our method to depth prediction on NYUDepth v2. We train using the entire NYUDepth v2 raw data distribution, using the scene split specified in the official train/test distribution. We then test on the common distribution depth maps, including filled-in areas, but constrained to the axis-aligned rectangle where there there is a valid depth map projection. Since the network output is a lower resolution than the original NYUDepth images, and excludes a small border, we bilinearly upsample our network outputs to the original 640x480 image scale, and extrapolate the missing border using a cross-bilateral filter. We compare our method to prior works Ladicky *et al.* [20],

[1] This shared model also enabled us to try enforcing compatibility between predicted normals and those obtained via finite difference of the predicted depth (predicting normals directly performs considerably better than using finite difference). However, while this constraint was able to improve the normals from finite difference, it failed to improve either task individually. Thus, while we make use of the shared model for computational efficiency, we do not use the extra compatibility constraint.

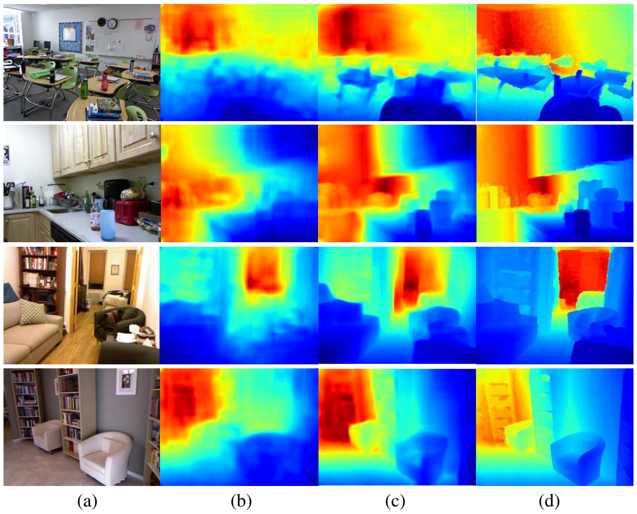

Figure 2. Example depth results. (a) RGB input; (b) result of [8]; (c) our result; (d) ground truth. Note the color range of each image is individually scaled.

Depth Prediction

	Ladicky[20]	Karsch[18]	Baig [1]	Liu [23]	Eigen[8]	Ours(A)	Ours(VGG)
$\delta < 1.25$	0.542	–	0.597	0.614	0.614	0.697	**0.769**
$\delta < 1.25^2$	0.829	–	–	0.883	0.888	0.912	**0.950**
$\delta < 1.25^3$	0.940	–	–	0.971	0.972	0.977	**0.988**
abs rel	–	0.350	0.259	0.230	0.214	0.198	**0.158**
sqr rel	–	–	–	–	0.204	0.180	**0.121**
RMS(lin)	–	1.2	0.839	0.824	0.877	0.753	**0.641**
RMS(log)	–	–	–	–	0.283	0.255	**0.214**
sc-inv.	–	–	0.242	–	0.219	0.202	**0.171**

Table 1. Depth estimation measurements. Note higher is better for top rows of the table, while lower is better for the bottom section.

Karsh *et al.* [18], Baig *et al.* [1], Liu *et al.* [23] and Eigen *et al.* [8].

The results are shown in Table 1. Our model obtains best performance in all metrics, due to our larger architecture and improved training. In addition, the VGG version of our model significantly outperforms the smaller AlexNet version, reenforcing the importance of model size; this is the case even though the depth task is seemingly far removed from the classification task with which the initial coarse weights were first trained. Qualitative results in Fig. 2 show substantial improvement in detail sharpness over [8].

6.2. Surface Normals

Next we apply our method to surface normals prediction. We compare against the 3D Primitives (3DP) and "Indoor Origami" works of Fouhey *et al.* [10, 11], Ladicky *et al.* [21], and Wang *et al.* [37]. As with the depth network, we used the full raw dataset for training, since ground-truth normal maps can be generated for all images. Since different systems have different ways of calculating ground truth normal maps, we compare using both the ground truth as constructed in [21] as well as the method used in [31]. The differences between ground truths are due primarily to the fact that [21] uses more aggressive smoothing; thus [21] tends to present flatter areas, while [31] is noisier but keeps more details present. We measure performance with the same metrics as in [10]: The mean and median angle from the ground truth across all unmasked pixels, as well as the percent of vectors whose angle falls within three thresholds.

Surface Normal Estimation (GT [21])

	Angle Distance		**Within t° Deg.**		
	Mean	**Median**	11.25°	22.5°	30°
3DP [10]	35.3	31.2	16.4	36.6	48.2
Ladicky *&al.* [21]	33.5	23.1	27.5	49.0	58.7
Fouhey *&al.* [11]	35.2	17.9	40.5	54.1	58.9
Wang *&al.* [37]	26.9	14.8	42.0	61.2	68.2
Ours (AlexNet)	23.7	15.5	39.2	62.0	71.1
Ours (VGG)	**20.9**	**13.2**	**44.4**	**67.2**	**75.9**

Surface Normal Estimation (GT [31])

	Angle Distance		**Within t° Deg.**		
	Mean	**Median**	11.25°	22.5°	30°
3DP [10]	37.7	34.1	14.0	32.7	44.1
Ladicky *&al.* [21]	35.5	25.5	24.0	45.6	55.9
Wang *&al.* [37]	28.8	17.9	35.2	57.1	65.5
Ours (AlexNet)	25.9	18.2	33.2	57.5	67.7
Ours (VGG)	**22.2**	**15.3**	**38.6**	**64.0**	**73.9**

Table 2. Surface normals prediction measured against the ground truth constructed by [21] (top) and [31] (bottom).

Results are shown in Table 2. The smaller version of our model performs similarly or slightly better than Wang *et al.*, while the larger version substantially outperforms all comparison methods. Figure 3 shows example predictions. Note the details captured by our method, such as the curvature of the blanket on the bed in the first row, sofas in the second row, and objects in the last row.

6.3. Semantic Labels

6.3.1 NYU Depth

We finally apply our method to semantic segmentation, first also on NYUDepth. Because this data provides a depth channel, we use the ground-truth depth and normals as input into the semantic segmentation network, as described in Section 4.3. We evaluate our method on semantic class sets with 4, 13 and 40 labels, described in [31], [6] and [13], respectively. The 4-class segmentation task uses high-level category labels "floor", "structure", "furniture" and "props", while the 13- and 40-class tasks use different sets of more fine-grained categories. We compare with several recent methods, using the metrics commonly used to evaluate each task: For the 4- and 13-class tasks we use pixel-wise and per-class accuracy; for the 40-class task, we also compare using the mean pixel-frequency weighted Jaccard index of each class, and the flat mean Jaccard index.

Results are shown in Table 3. We decisively outperform the comparison methods on the 4- and 14-class tasks. In the 40-class task, our model outperforms Gupta *et al.* '14 with both model sizes, and Long *et al.* with the larger size. Qualitative results are shown in Fig. 4. Even though our method does not use superpixels or any piecewise constant assumptions, it nevertheless tends to produce large constant regions most of the time.

4-Class Semantic Segmentation	Pixel	Class
Couprie *&al.* [6]	64.5	63.5
Khan *&al.* [15]	69.2	65.6
Stuckler *&al.* [33]	70.9	67.0
Mueller *&al.* [26]	72.3	71.9
Gupta *&al.* '13 [13]	78	–
Ours (AlexNet)	80.6	79.1
Ours (VGG)	**83.2**	**82.0**

13-Class Semantic	Pixel	Class
Couprie *&al.* [6]	52.4	36.2
Wang *&al.* [37]	–	42.2
Hermans *&al.* [17]	54.2	48.0
Khan *&al.* [15] *	58.3	45.1
Ours (AlexNet)	70.5	59.4
Ours (VGG)	**75.4**	**66.9**

40-Class Semantic Segmentation	Pix. Acc.	Per-Cls Acc.	Freq. Jaccard	Av. Jaccard
Gupta*&al.*'13 [13]	59.1	28.4	45.6	27.4
Gupta*&al.*'14 [14]	60.3	35.1	47.0	28.6
Long*&al.* [24]	65.4	**46.1**	49.5	34.0
Ours (AlexNet)	62.9	41.3	47.6	30.8
Ours (VGG)	**65.6**	45.1	**51.4**	**34.1**

Table 3. Semantic labeling on NYUDepth v2

* Khan*&al.* use a different overlapping label set.

Sift Flow Semantic Segmentation	Pix. Acc.	Per-Class Acc.	Freq. Jacc	Av. Jacc
Farabet *&al.* (1) [9]	78.5	29.6	–	–
Farabet *&al.* (2) [9]	74.2	46.0	–	–
Tighe *&al.* [35]	78.6	39.2	–	–
Pinheiro *&al.* [28]	77.7	29.8	–	–
Long *&al.* [24]	85.1	51.7	76.1	**39.5**
Ours (AlexNet) (1)	84.0	42.0	73.7	33.1
Ours (AlexNet) (2)	81.6	48.2	71.3	32.6
Ours (VGG) (1)	**86.8**	46.4	**77.9**	38.8
Ours (VGG) (2)	83.8	**55.7**	74.7	37.6

Table 4. Semantic labeling on the Sift Flow dataset. (1) and (2) correspond to non-reweighted and class-reweighted versions of our model (see text).

Pascal VOC Semantic Segmentation	2011 Validation				2011 Test	2012 Test
	Pix. Acc.	Per-Cls Acc.	Freq.Jacc	Av.Jacc	Av.Jacc	Av.Jacc
Dai*&al.*[7]	–	–	–	–	–	61.8
Long*&al.*[24]	90.3	75.9	83.2	62.7	**62.7**	62.2
Chen*&al.*[5]	–	–	–	–	–	**71.6**
Ours (VGG)	90.3	72.4	82.9	62.2	62.5	62.6

Table 5. Semantic labeling on Pascal VOC 2011 and 2012.

Contributions of Scales	**Depth**	**Normals**	**4-Class**		**13-Class**	
			RGB+D+N	RGB	RGB+D+N	RGB
	Pixelwise Error lower is better		Pixelwise Accuracy higher is better			
Scale 1 only	0.218	29.7	71.5	71.5	58.1	58.1
Scale 2 only	0.290	31.8	77.4	67.2	65.1	53.1
Scales 1 + 2	0.216	26.1	80.1	74.4	69.8	63.2
Scales 1 + 2 + 3	0.198	25.9	80.6	75.3	70.5	64.0

Table 6. Comparison of networks for different scales for depth, normals and semantic labeling tasks with 4 and 13 categories. Largest single contributing scale is underlined.

6.3.2 Sift Flow

We confirm our method can be applied to additional scene types by evaluating on the Sift Flow dataset [22], which contains images of outdoor cityscapes and landscapes segmented into 33 categories. We found no need to adjust convolutional kernel sizes or learning rates for this dataset, and simply transfer the values used for NYUDepth directly; however, we do adjust the output sizes of the layers to match the new image sizes.

We compare against Tighe *et al.* [35], Farabet *et al.* [9], Pinheiro [28] and Long *et al.* [24]. Note that Farabet *et al.* train two models, using empirical or rebalanced class distributions by resampling superpixels. We train a more class-balanced version of our model by reweighting each class in the cross-entropy loss; we weight each pixel by $\alpha_c = median\_freq / freq(c)$ where $freq(c)$ is the number of pixels of class c divided by the total number of pixels in images where c is present, and $median\_freq$ is the median of these frequencies.

Results are in Table 4; we compare regular (1) and reweighted (2) versions of our model against comparison methods. Our smaller model substantially outperforms all but Long *et al.* , while our larger model performs similarly to Long *et al.* This demonstrates our model's adaptability not just to different tasks but also different data.

6.3.3 Pascal VOC

In addition, we also verify our method using Pascal VOC. Similarly to Long *et al.* [24], we train using the 2011 training set augmented with 8498 training images collected by Hariharan *et al.* [16], and evaluate using the 736 images from the 2011 validation set not also in the Hariharan extra set, as well as on the 2011 and 2012 test sets. We perform online data augmentations as in our NYUDepth and Sift Flow models, and use the same learning rates. Because these images have arbitrary aspect ratio, we train our model on square inputs, and scale the smaller side of each image to 256; at test time we apply the model with a stride of 128 to cover the image (two applications are usually sufficient).

Results are shown in Table 5 and Fig. 5. We compare with Dai *et al.* [7], Long *et al.* [24] and Chen *et al.* [5]; the latter is a more recent work that augments a convolutional network with large top-layer field of and fully-connected CRF. Our model performs comparably to Long *et al.*, even as it generalizes to multiple tasks, demonstrated by its adeptness at depth and normals prediction.

7. Probe Experiments

7.1. Contributions of Scales

We compare performance broken down according to the different scales in our model in Table 6. For depth, normals and 4- and 13-class semantic labeling tasks, we train and evaluate the model using just scale 1, just scale 2, both, or all three scales 1, 2 and 3. For the coarse scale-1-only prediction, we replace the last fully connected layer of the coarse stack with a fully connected layer that outputs directly to target size, *i.e.* a pixel map of either 1, 3, 4 or 13 channels depending on the task. The spatial resolution is the same as is used for the coarse features in our model, and is upsampled in the same way.

We report the "abs relative difference" measure (*i.e.* $|D - D^*|/D^*$) to compare depth, mean angle distance for normals, and pixelwise accuracy for semantic segmentation.

First, we note there is progressive improvement in all tasks as scales are added (rows 1, 3, and 4). In addition, we find the largest single contribution to performance is the

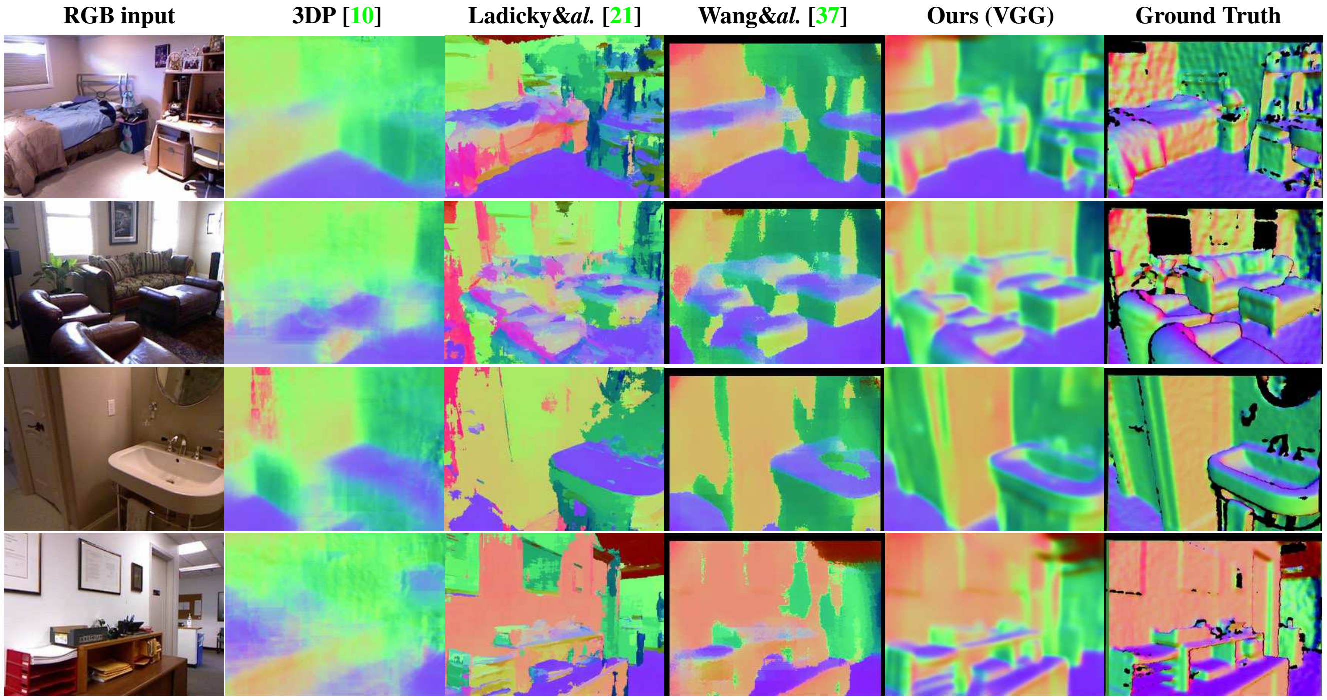

Figure 3. Comparison of surface normal maps.

Effect of Depth/Normals Inputs

	Scale 2 only		Scales 1 + 2	
	Pix. Acc.	Per-class	Pix. Acc.	Per-class
RGB only	53.1	38.3	63.2	50.6
RGB + pred. D&N	58.7	43.8	65.0	49.5
RGB + g.t. D&N	65.1	52.3	69.8	58.9

Table 7. Comparison of RGB-only, predicted depth/normals, and ground-truth depth/normals as input to the 13-class semantic task.

coarse Scale 1 for depth and normals, but the more local Scale 2 for the semantic tasks — however, this is only due to the fact that the depth and normals channels are introduced at Scale 2 for the semantic labeling task. Looking at the labeling network with RGB-only inputs, we find that the coarse scale is again the larger contributer, indicating the importance of the global view. (Of course, this scale was also initialized with ImageNet convolution weights that are much related to the semantic task; however, even initializing randomly achieves 54.5% for 13-class scale 1 only, still the largest contribution, albeit by a smaller amount).

7.2. Effect of Depth and Normals Inputs

The fact that we can recover much of the depth and normals information from the RGB image naturally leads to two questions: (*i*) How important are the depth and normals inputs relative to RGB in the semantic labeling task? (*ii*) What might happen if we were to replace the true depth and normals inputs with the predictions made by our network?

To study this, we trained and tested our network using either Scale 2 alone or both Scales 1 and 2 for the 13-class semantic labeling task under three input conditions: (*a*) the RGB image only, (*b*) the RGB image along with predicted depth and normals, or (*c*) RGB plus true depth and normals. Results are in Table 7. Using ground truth depth/normals shows substantial improvements over RGB alone. Predicted depth/normals appear to have little effect when using both scales, but a tangible improvement when using only Scale 2. We believe this is because any relevant information provided by predicted depths/normals for labeling can also be extracted from the input; thus the labeling network can learn this same information itself, just from the label targets. However, this supposes that the network structure is capable of learning these relations: If this is not the case, *e.g.* when using only Scale 2, we do see improvement. This is also consistent with Section 7.1, where we found the coarse network was important for prediction in all tasks — indeed, supplying the predicted depth/normals to scale 2 is able to recover much of the performance obtained by the RGB-only scales 1+2 model.

8. Discussion

Together, depth, surface normals and semantic labels provide a rich account of a scene. We have proposed a simple and fast multiscale architecture using convolutional networks that gives excellent performance on all three modalities. The models beat existing methods on the vast majority of benchmarks we explored. This is impressive given that many of these methods are specific to a single modality and often slower and more complex algorithms than ours. As such, our model provides a convenient new baseline for the three tasks. To this end, code and trained models can be found at `http://cs.nyu.edu/~deigen/dnl/`.

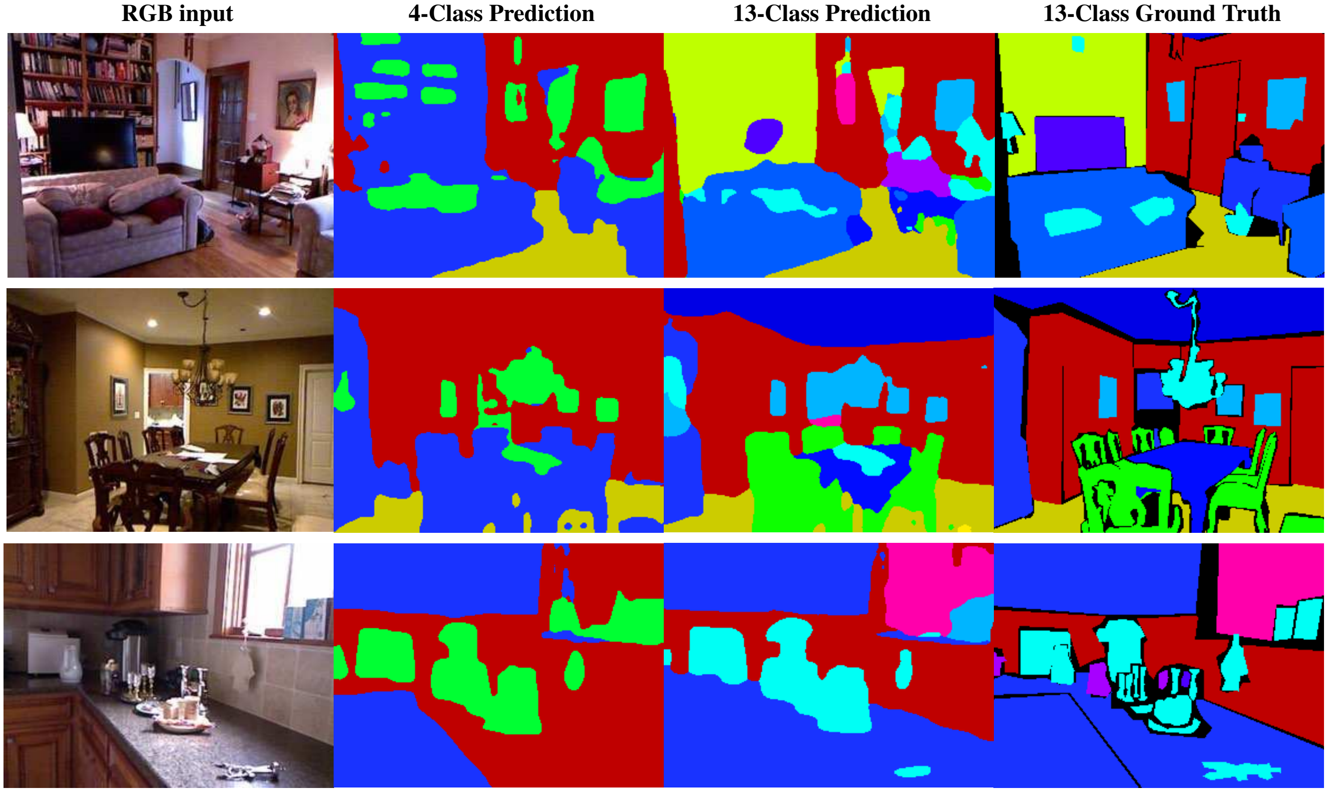

Figure 4. Example semantic labeling results for NYUDepth: (a) input image; (b) 4-class labeling result; (c) 13-class result; (d) 13-class ground truth.

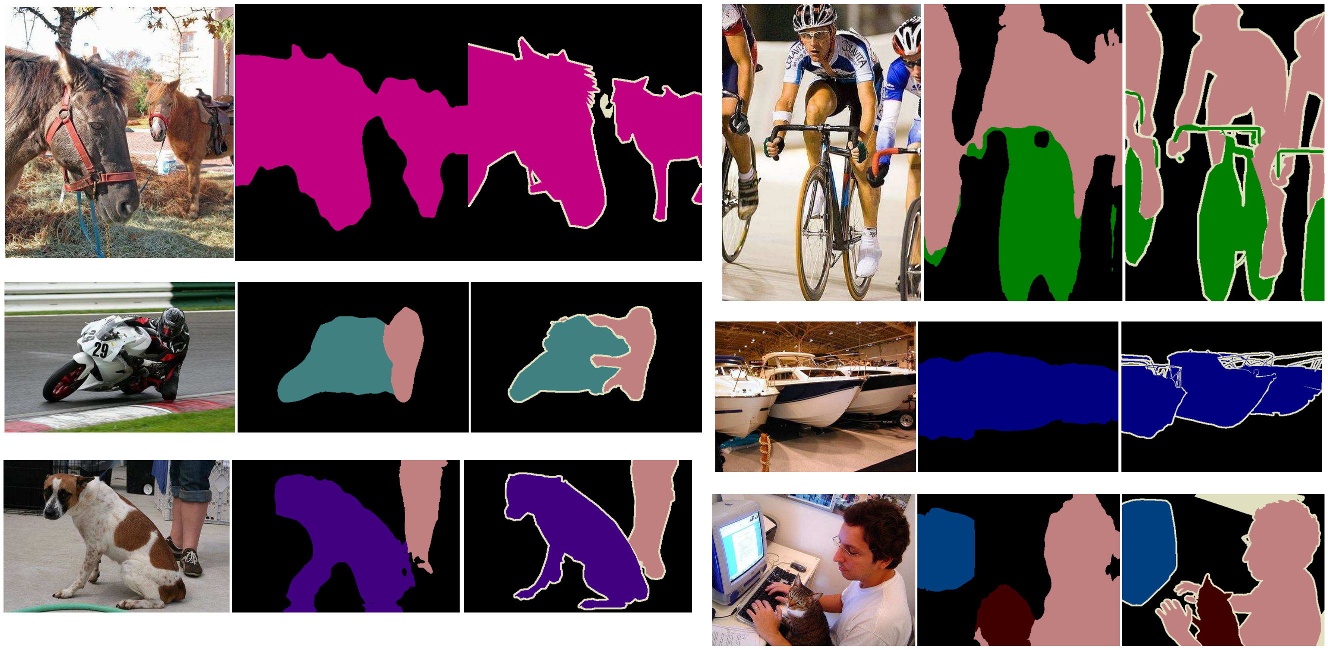

Figure 5. Example semantic labeling results for Pascal VOC 2011. For each image, we show RGB input, our prediction, and ground truth.

Acknowledgements

This work was supported by an ONR #N00014-13-1-0646 and an NSF CAREER grant.

References

[1] M. H. Baig and L. Torresani. Coarse-to-fine depth estimation from a single image via coupled regression and dictionary learning. *arXiv:1501.04537*, 2015. 5

[2] J. T. Barron and J. Malik. Intrinsic scene properties from a single rgb-d image. *CVPR*, 2013. 1, 2

[3] J. T. Barron and J. Malik. Shape, illumination, and reflectance from shading. *TPAMI*, 2015. 1, 2

[4] J. Carreira and C. Sminchisescu. Cpmc: Automatic object segmentation using constrained parametric min-cuts. *PAMI*, 2012. 2

[5] L.-C. Chen, G. Papandreou, I. Kokkinos, K. Murphy, and A. L. Yuille. Semantic image segmentation with deep convolutional nets and fully connected crfs. *ICLR*, 2015. 6

[6] C. Couprie, C. Farabet, L. Najman, and Y. LeCun. Indoor semantic segmentation using depth information. *ICLR*, 2013. 2, 3, 5, 6

[7] J. Dai, K. He, and J. Sun. Convolutional feature masking for joint object and stuff segmentation. *arXiv 1412.1283*, 2014. 6

[8] D. Eigen, C. Puhrsch, and R. Fergus. Depth map prediction from a single image using a multi-scale deep network. *NIPS*, 2014. 1, 3, 5

[9] C. Farabet, C. Couprie, L. Najman, and Y. LeCun. Scene parsing with multiscale feature learning, purity trees, and optimal covers. *arXiv:1202.2160*, 2012. 2, 3, 6

[10] D. F. Fouhey, A. Gupta, and M. Hebert. Data-driven 3d primitives for single image understanding. In *ICCV*, 2013. 1, 5, 7

[11] D. F. Fouhey, A. Gupta, and M. Hebert. Unfolding an indoor origami world. In *ECCV*, 2014. 1, 2, 5

[12] R. B. Girshick, J. Donahue, T. Darrell, and J. Malik. Rich feature hierarchies for accurate object detection and semantic segmentation. *CVPR*, 2014. 1

[13] S. Gupta, P. Arbelaez, and J. Malik. Perceptual organization and recognition of indoor scenes from rgb-d images. In *CVPR*, 2013. 2, 5, 6

[14] S. Gupta, R. Girshick, P. Arbeláez, and J. Malik. Learning rich features from rgb-d images for object detection and segmentation. In *ECCV*. 2014. 1, 2, 4, 6

[15] S. K. Hameed, M. Bennamoun, F. Sohel, and R. Togneri. Geometry driven semantic labeling of indoor scenes. In *ECCV*. 2014. 2, 6

[16] B. Hariharan, P. Arbeláez, R. Girshick, and J. Malik. Simultaneous detection and segmentation. In *ECCV*. 2014. 6

[17] A. Hermans, G. Floros, and B. Leibe. Dense 3d semantic mapping of indoor scenes from rgb-d images. *ICRA*, 2014. 2, 6

[18] K. Karsch, C. Liu, S. B. Kang, and N. England. Depth extraction from video using non-parametric sampling. In *TPAMI*, 2014. 5

[19] A. Krizhevsky, I. Sutskever, and G. Hinton. Imagenet classification with deep convolutional neural networks. In *NIPS*, 2012. 1, 3

[20] L. Ladicky, J. Shi, and M. Pollefeys. Pulling things out of perspective. In *CVPR*, 2014. 4, 5

[21] L. Ladicky, B. Zeisl, and M. Pollefeys. Discriminatively trained dense surface normal estimation. 1, 5, 7

[22] C. Liu, J. Yuen, A. Torralba, J. Sivic, and W. Freeman. Sift flow: dense correspondence across difference scenes. 2008. 6

[23] F. Liu, C. Shen, and G. Lin. Deep convolutional neural fields for depth estimation from a single image. *arXiv:1411.6387*, 2014. 5

[24] J. Long, E. Shelhamer, and T. Darrell. Fully convolutional networks for semantic segmentation. *CoRR*, abs/1411.4038, 2014. 2, 6

[25] R. Memisevic and C. Conrad. Stereopsis via deep learning. In *NIPS Workshop on Deep Learning*, 2011. 1

[26] A. C. Muller and S. Behnke. Learning depth-sensitive conditional random fields for semantic segmentation of rgb-d images. *ICRA*, 2014. 2, 6

[27] M. Osadchy, Y. Le Cun, and M. L. Miller. Synergistic face detection and pose estimation with energy-based models. In *Toward Category-Level Object Recognition*, pages 196–206. Springer, 2006. 1

[28] P. Pinheiro and R. Collobert. Recurrent convolutional neural networks for scene labeling. In *ICML*, 2014. 2, 6

[29] X. Ren, L. Bo, and D. Fox. Rgb-(d) scene labeling: Features and algorithms. In *CVPR*, 2012. 2

[30] P. Sermanet, D. Eigen, X. Zhang, M. Mathieu, R. Fergus, and Y. LeCun. Overfeat: Integrated recognition, localization and detection using convolutional networks. *ICLR*, 2013. 1

[31] N. Silberman, D. Hoiem, P. Kohli, and R. Fergus. Indoor segmentation and support inference from rgbd images. In *ECCV*, 2012. 2, 4, 5

[32] K. Simonyan and A. Zisserman. Very deep convolutional networks for large-scale image recognition. *CoRR*, abs/1409.1556, 2014. 1, 2, 3

[33] J. Stuckler, B. Waldvogel, H. Schulz, and S. Behnke. Dense real-time mapping of object-class semantics from rgb-d video. *J. Real-Time Image Processing*, 2014. 6

[34] C. Szegedy, W. Liu, Y. Jia, P. Sermanet, S. Reed, D. Anguelov, D. Erhan, V. Vanhoucke, and A. Rabinovich. Going deeper with convolutions. *CoRR*, abs/1409.4842, 2014. 1

[35] J. Tighe and S. Lazebnik. Finding things: Image parsing with regions and per-exemplar detectors. In *CVPR*, 2013. 2, 6

[36] J. Tompson, A. Jain, Y. LeCun, and C. Bregler. Joint training of a convolutional network and a graphical model for human pose estimation. *NIPS*, 2014. 1

[37] A. Wang, J. Lu, G. Wang, J. Cai, and T.-J. Cham. Multimodal unsupervised feature learning for rgb-d scene labeling. In *ECCV*. 2014. 1, 2, 5, 6, 7

[38] J. Zbontar and Y. LeCun. Computing the stereo matching cost with a convolutional neural network. *CoRR*, abs/1409.4326, 2014. 1